

Extremum-seeking control for an Ultrasonic/Sonic Driller/Corer (USDC) driven at high-power

Jack Aldrich, Stewart Sherrit, Xiaoqi Bao, Yoseph Bar-Cohen, Mircea Badescu, Zensheu Chang

JPL/Caltech, (MS 67-119), 4800 Oak Grove Drive, Pasadena, CA 91109-8099,

ABSTRACT

Future NASA exploration missions will increasingly require sampling, in-situ analysis and possibly the return of material to Earth for further tests. One of the challenges to addressing this need is the ability to drill using for low axial loading while operating from light weight platforms (e.g., lander, rover, etc.) as well as operate at planets with low gravity. For this purpose, the authors developed the Ultrasonic/Sonic Driller/Corer (USDC) jointly with Cybersonics Inc. Studies of the operation of the USDC at high power have shown there is a critical need to self-tune to maintain the operation of the piezoelectric actuator at resonance. Performing such tuning is encountered with difficulties and to address them an extremum-seeking control algorithm is being investigated. This algorithm is designed to tune the driving frequency of a time-varying resonating actuator subjected to both random and high-power impulsive noise disturbances. Using this algorithm the performance of the actuator is monitored on a time-scale that is compatible with its slowly time-varying physical characteristics. The algorithm includes a parameter estimator, which estimates the coefficients of a function that characterizes the quality factor of the USDC. Since the parameter estimator converges sufficiently faster than the time-varying drift of the USDC's physical parameters, the proposed extremum-seeking estimation and control algorithm is potentially applicable for use as a closed-loop health monitoring system. Specifically, this system may be programmed to automatically adjust the duty-cycle of the sinusoidal driver signal to guarantee that the quality factor of the USDC does not fall below a user-defined set-point. Such fault-tolerant functionality is especially important in automated drilling applications where it is essential not to inadvertently drive the piezoelectric ceramic crystals of the USDC beyond their capacities. The details of the algorithm and experimental results will be described and discussed in this paper.

Keywords: High-power piezoelectric actuator, Ultrasonic/Sonic Driller/Corer, Peak-seeking estimation and control

1. INTRODUCTION

Future NASA exploration missions to Mars, Europa, Titan, comets and asteroids are seeking to perform sampling, in-situ analysis and possibly the return of material to Earth for further tests. Existing drilling techniques are limited by the need for large axial forces and holding torques, high power consumption and an inability to efficiently duty cycle. Lightweight robots and rovers have difficulties accommodating these requirements. To address these key challenges to the NASA objective of planetary in-situ rock sampling and analysis, an ultrasonic/sonic driller/corer (USDC) was developed [Bar-Cohen et al, 2001; Sherrit et al, 2000].



Figure 1 - USDC drilling

The actuator of the USDC is an ultrasonic horn transducer that is driven by a piezoelectric stack. Unlike the typical ultrasonic drill where the drill stem is acoustically coupled to the transducer, the horn transducer in the USDC drives a free flying mass (free-mass), which bounces between the horn tip and a drill stem at sonic frequencies. The impacts of the free-mass create stress pulses that propagate to the interface of the stem tip and the rock. The rock fractures when its ultimate strain is exceeded at the rock/bit interface. This novel drilling mechanism has been shown to be more efficient and versatile than conventional ultrasonic drills under a variety of conditions. The low mass of a USDC device and the ability to operate with minimum axial load with near zero holding torque (see Fig. 1) offers an important tool for sample acquisition and in-situ analysis. Another important characteristic of the USDC is the capability to operate in the restrictive space environment.

The functionality of the USDC was modeled to predict its performance. The developed model describes five elements involved in the drilling i.e. the electrical driver, ultrasonic transducer, free-mass, drill stem, and the rock. In a previous publication the main elements and the interaction between them were analyzed and modeled separately [Bao et.al. 2003]. A one-dimensional model was then developed for each interaction and an integrated software program was developed to simulate the operation of all parts of the USDC. This paper presents the modeling and control design.

2. MODELING

The USDC device consists of three main parts: an ultrasonic transducer (piezoelectric stack, a backing element, and a horn), a free-mass, and a drill stem. Fig. 2 shows a schematic of the USDC device. The ultrasonic/sonic transducer can be designed to vibrate at a frequency from 5 to 25kHz depending on the application. The vibrations of the horn tip excite the free-mass, causing it to bounce between the horn tip and the top of the drill stem with an average frequencies in the range of 100 to 1000 Hz. The free-mass transfers energy from the ultrasonic transducer to the drill stem. The shock waves caused by the impacts of the free-mass on the drill bit propagate to the bit/rock interface and wherever the rock is strained past its ultimate strain it fractures. In order to determine the critical issues related to the control and optimization of the drill, models of the interaction at the various interfaces of the drill have been investigated. The four interactions that were modeled include: 1) transducer with the driving circuit, 2) horn tip with the free-mass, 3) free-mass with the drill stem and 4) base of the drill stem (bit) with the rock. Thus analysis has been presented in detail in a previous paper [Bao et al, 2003]. The following is a brief review of items 1 and 2. From this analysis, a relevant control objective is defined. Practical issues in achieving the control objective will be discussed in subsequent sections. A software package was developed to analyze the closed-loop performance of various designs of a USDC device for ice coring, and these results are presented in the accompanying paper [Mircea's paper].

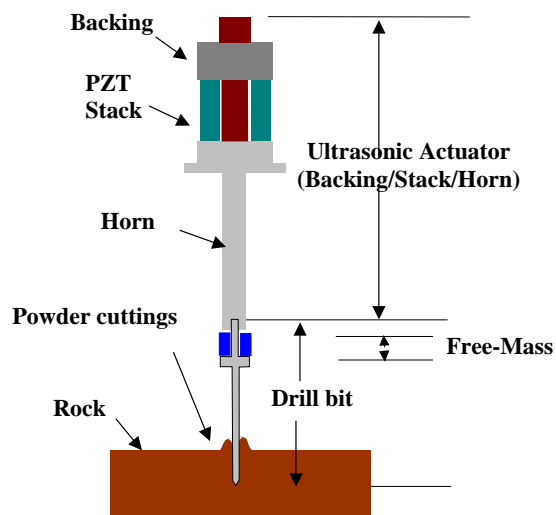


Figure 2 - USDC schematics

2.1. Transducer/ ultrasonic actuator

The transducer/ultrasonic actuator consists of a PZT-8 stack maintained in compression between a horn and a backing by a pre-stress bolt. The horn amplifies the vibration amplitude by varying the cross-sectional along its length. Various shapes of the horn were analyzed, including a dog-bone horn, a solid horn and a stepped horn. The transducer is a composite longitudinal vibrator with varying cross sections and can be modeled by the Mason equivalent circuit as presented in a previous paper [Sherrit et al, 1999]. In order to include engineering details in the final transducer design the finite element approach was used to determine the full frequency response of this piezoelectric device. An electromechanically coupled element [Allik and Hughes, 1970] was applied to model the piezoelectric material, which is available in commercial software ANSYSTM.

In this high power ultrasonic application, the transducer is designed and fabricated to have high mechanical Q, and is operated at or near its first longitudinal resonance frequency. Using modal analysis allowed us to isolate and concentrate on this resonance mode and it simplifies the model and reduces the computing time. Solving the generalized eigenvalue problem of finite element equations, the resonance frequencies and corresponding mode shapes can be found. We obtain a set of resonance frequencies, $\omega_1, \omega_2, \dots, \omega_n$ and normalized mode shapes (eigenvectors)

$$\{\xi_1\}, \{\xi_2\}, \dots, \{\xi_n\}. \quad (1)$$

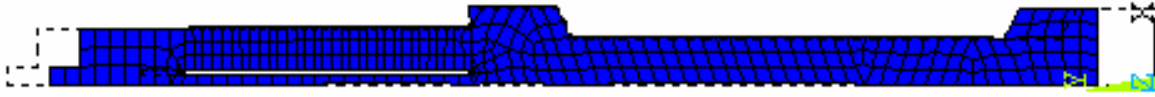


Figure 3 - Mode shape

Fig. 3 shows the modal shape of the first nonzero-frequency resonance of the transducer calculated by ANSYSTM. The mode is basically a longitudinal vibration with larger displacement at the horn tip (right hand side in Fig. 3) than at the back. The calculated resonance frequency was found to be 5.275 kHz using the material property data provided by the manufacturers, which was very close to the measured resonance frequency located between 5.2 to 5.3 kHz.

By expressing the displacement as the summation of the modal shapes as:

$$\{\xi\} = \sum_n d_i \{\xi_i\} \quad (2)$$

The finite equations can be converted to modal equations and be simplified to an equivalent circuit for convenience in computation as was reported in a previous work [Bao et al, 2003],

$$\begin{aligned} (\omega_i^2 + j\omega R_i - \omega^2)d_i &= p_i V + Fm_i \\ Q &= \sum_n p_i d_i + C_0 V \end{aligned} \quad i=1, \dots, n \quad (3)$$

where d_i is the amplitude of the mode i , Q is the electric charge on the electrode, R_i , p_i and Fm_i are effective damping, electromechanical coupling and force for the modes respectively. The R_i and p_i can be calculated from the finite element matrixes, and Fm_i is expressed as

$$Fm_i = \{\xi_i\}^T \{F\}, \quad (4)$$

where $\{F\}$ is the vector of the force applied on the nodes.

Only the first longitudinal mode is taken into account in the analysis. With these substitutions (3) becomes:

$$\begin{aligned} (\omega_1^2 + j\omega R - \omega^2)d &= pV + Fm \\ Q &= pd + C_0 V \end{aligned} \quad (5)$$

where subscripts are omitted for simplification.

A further simplification is shown for (5) by representing the response of the device by an equivalent circuit around resonance as is shown in Fig. 4, where subscripts m are added to denote that the symbols actually represent mechanical variables and parameters. The element in the dashed square is the sketch of the electric driving circuit.

Upon inspection we have $L_m = 1$, $C_m = 1/\omega_i^2$ and the mechanical "current" I_m is the modal velocity

$$I_m = \dot{d}. \quad (6)$$

The mechanical resistance R_m is determined experimentally. When the transducer is driven electrically and is mechanically unconstrained (no impacts with the free-mass), the modal velocity can be shown to be

$$I_m = \frac{pV}{j(\omega L_m - \frac{1}{\omega C_m}) + R_m} \quad (7)$$

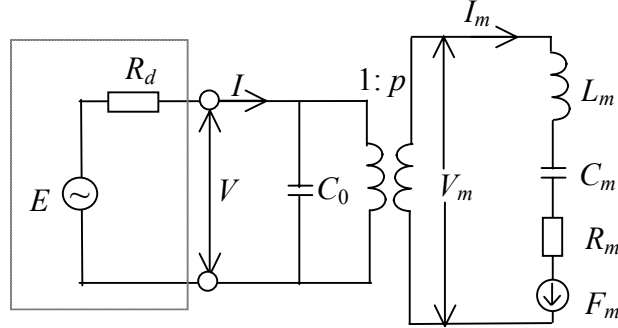


Figure 4 - Schematic of the equivalent circuit of the transducer around resonance. The generator source is also included in the dashed square.

2.1.1. Reaction of free-mass impacts to the transducer

In the operation of the USDC, a small preload force, either from gravity or from a spring is applied to the transducer to close the gap between the horn tip and the free mass. The force pushes the transducer down toward the free-mass and the bit. A harmonic voltage at a frequency around the resonance drives the transducer. The free-mass, energized by the impacts with the vibrating horn tip, then, bounces between the bit and horn tip and maintains a gap between them. The impacts of the free-mass to the horn tip affect both vibration and translation movements of the horn transducer.

a) Translation movement of the horn transducer

We assume the preload force is constant and produces an acceleration a of the transducer. Suppose an impact happens at time t_I , and contact time is very short, the contact force can be expressed as

$$F_c = f_I \delta(t - t_I) \quad (8)$$

where δ is the delta function. Using momentum conservation in the impact, we have

$$f_I = -m \Delta v_I \quad (9)$$

where m is the mass and Δv_I is the change in free-mass speed before and after impact. Each impact results in a change of the center of mass (COM) velocity of the horn by

$$\Delta U_I = \frac{-m \Delta v_I}{M} H(t - t_I) \quad (10)$$

where M is the total mass of the horn transducer, and H is the step function. Therefore, the COM velocity of the transducer becomes

$$U = U_0 + at + \sum_I \Delta U_I \quad (11)$$

Due to the fact that the average velocity of the transducer is zero,

$$\lim_{T \rightarrow \infty} \frac{1}{T} \int_0^T U(t) dt = 0 \quad (12)$$

the average of Δv_I over all impacts in I , denoted Δv_{av} , can be computed from (10-12) as follows

$$\Delta v_{av} = \lim_{|I| \rightarrow \infty} \frac{1}{|I|} \sum_I \Delta v_I = \frac{a T_{av} M}{m} \quad (12b)$$

where T_{av} denotes the average time elapsed between consecutive impacts between the horn and the free-mass.

b) Vibration of the transducer with constant harmonic voltage driving

When the source resistance R_d , as shown in Fig. 3, is zero the transducer is driven by a constant voltage. In this case, the vibration of the transducer can be solved explicitly. From the equivalent circuit, we can write the corresponding differential equation as

$$L_m \ddot{d} + R_m \dot{d} + C_m d = pV + F_m \quad (13)$$

The solution of this equation is the summation of the vibration induced by the electric voltage V and the vibration caused by the mechanical force F_m . The steady solution for a harmonic voltage $V = V_0 \exp(j\omega t)$ is

$$I_{me} = \dot{d}_e = \frac{pV}{j(\omega L_m - 1/\omega C_m) + R_m} \quad (14)$$

A mechanical force is caused by the impacts of the free-mass on the horn tip and can be determined from (4), (8) and (9), to be

$$F_m = \xi_t f_I \delta(t - t_I) = -m\Delta v_I \xi_t \delta(t - t_I) \quad (15)$$

where ξ_t is the tip displacement of the mode shape. The time-averaged mechanical force caused by the impacts is

$$\lim_{T \rightarrow \infty} \frac{1}{T} \int_0^T F_m(t) dt = -m\Delta v_{av} \xi_t \lim_{T \rightarrow \infty} \frac{1}{T} \int_0^T \delta(t - t_I) dt = \frac{-m\Delta v_{av} \xi_t}{T_{av}} = -aM \xi_t \quad (15b)$$

The solution of (12) for the impact force F_m is a free ring-down vibration after the impact time t_I and is expressed as

$$I_{ml} = \dot{d}_I = -\frac{m\Delta v_I \xi_t}{L_m} \exp[(-\alpha + j\omega_f)(t - t_I)] \quad (16)$$

where α is the damping coefficient and ω_f is the free vibration frequency, and

$$\alpha = -\frac{R_m}{2L_m} \quad (16b)$$

$$\omega_f = \sqrt{\omega_1^2 - (R_m / 2L_m)^2} \quad (17)$$

The final solution of the modal velocity is

$$I_m = \dot{d} = \dot{d}_e + \sum_I \dot{d}_I = I_{me} + \sum_I I_{ml} \quad (18)$$

Assumption. For modeling purposes, we assume that the affect of the impact forces F_m can be accounted for by adjusting the circuit's average impedance.

c) Transducer driven by a driver with output resistance

In general, the output resistance of electronic drivers is not zero. The resistance will reduce the output voltage, increase energy loss and change the characteristics of the vibrations induced by the impacts.

The same approach utilized in the previous section can be applied to the case of non-zero output impedances of the drive circuit except resulting more complicated solution. The steady solution of the electric driving voltage in this case is then

$$I_{me} = \dot{d}_e = \frac{pEZ_x / (R_d + Z_x)}{j(\omega L_m - 1/\omega C_m) + R_m} \quad (19)$$

where the impedance of the transducer Z_x is

$$Z_x = \frac{j(\omega L_m - 1/\omega C_m) + R_m}{j\omega C_0 [j(\omega L_m - 1/\omega C_m) + R_m] + 1/p^2} \quad (20)$$

The solution for the impact is

$$I_{ml} = \dot{d}_l = -\frac{m\Delta v \xi_t}{L_m} \exp[S(t-t_l)] \quad (21)$$

where S is the solution of

$$L_m C_m R_d C_0 S^3 + (L_m C_m + R_m C_m R_d C_0) S^2 + (R_m C_m + p^2 R_d C_m + R_d C_0) S + 1 = 0 \quad (22)$$

This cubic equation has one real root and a pair of conjugate complex roots. For the free attenuating vibration, the solution S is in the form as

$$S = -\alpha + j\omega_f. \quad (23)$$

Although it is possible to obtain explicit expression of the solution, the expression is cumbersome and not accurate in practical numerical calculations.

d) Interaction between the transducer and the electric driver

Power output from the voltage source P_E is the time averaged integral of product of multiplication of the source voltage by the current and is expressed as

$$\begin{aligned} P_E &= \frac{1}{T} \int_T E(t) I(t) dt \\ &= \frac{1}{T} \int_T E(t) I_e(t) dt + \frac{1}{T} \int_T E(t) \sum_I I_I(t) dt \end{aligned} \quad (24)$$

or

$$P_E = P_{Ee} + P_{EI}, \quad (25)$$

where the first item in (24), P_{Ee} , is the power with no free-mass loading and is the power change introduced by the free-mass loading. $I_e(t)$ is the current through the source due to the electric drive voltage, and $I_I(t)$ is the current due to the free-mass impacts,

$$I_e(t) = \text{Re}\left(\frac{E}{Z_x(\omega) + R_d}\right) \quad (26)$$

$$I_I(t) = \text{Re}\left(\frac{pI_{ml}}{j\omega_f C_0 R_d + 1}\right). \quad (27)$$

The power lost on the resistor P_d is calculated using the time-averaged power

$$P_d = \frac{1}{T} \int_T R_d [I(t)]^2 dt = \frac{R_d}{T} \int_T [I_e(t) + \sum_I I_I(t)]^2 dt \quad (28)$$

It should be noted that, in these power calculations, all voltages and currents are expressed as real functions of time rather than their complex expression. Beside, the currents introduced by the impacts $I_I(t)$ attenuate with time and oscillate at the frequency ω_f , which may be different from the driving frequency ω . Therefore, the integrals in (24) and (28) are in a general form of

$$Int = \int \cos(at + f) \cos(bt + g) e^{-ct} dt. \quad (29)$$

e) Time-averaged vibration of the transducer under constant harmonic voltage and time-averaged impacts

A mechanical force is caused by the impacts of the free-mass on the horn tip and can be determined from (15), to be

$$\lim_{T \rightarrow \infty} \frac{1}{T} \int_0^T F_m(t) dt = -m\Delta v_{av} \xi_t \lim_{T \rightarrow \infty} \frac{1}{T} \int_0^T \delta(t-t_l) dt = \frac{-m\Delta v_{av} \xi_t}{T_{av}} = -aM\xi. \quad (30)$$

2.2. Model-based control objective

From figure 4, the complex electrical admittance of the transducer/ultrasonic actuator, denoted Y_x , is governed by

$$Y_x = pY_m + j\omega C_0, \quad (35)$$

where Y_m is the voltage-to-velocity transfer function of the mechanical resonator given by

$$Y_m = \frac{p}{j(\omega L_m - 1/\omega C_m) + R_m} \quad (36)$$

In order to maximize drilling rates, the control objective is to determine the sinusoidal drive frequency ω that maximizes $|Y_m(\omega)|$. If L_m and C_m are known, then the optimal control law ω^* becomes

$$\omega^* = \omega_1 = \frac{1}{\sqrt{L_m C_m}} \quad (37)$$

However, L_m and C_m are temperature-dependent parameters that are not known precisely. Viewing these parameters as unknown time-varying quantities motivates the following tracking control problem.

$$\max_{\omega} |Y_m(\omega, t)| = \max_{\omega} \frac{|I_m(\omega, t)|}{|V(\omega, t)|} \quad (38)$$

If the drive voltage amplitude $|V|$ and the horn tip's modal velocity amplitude $|I_m|$ are measurements available in real-time, then resonance tracking amounts to continuously updating the drive frequency ω to take steps in the direction of steepest ascent of $|Y_m(\omega)|$. This algorithm is straightforward and will be addressed in the next section. Unfortunately, the horn tip's modal velocity amplitude $|I_m|$ is not an available measurement. However, the electrical current going into the transducer is measurable using a low-resistance resistor. Hence, the following sub-optimal, yet practical, control problem is implementable

$$\max_{\omega} |Y_x(\omega, t)| = \max_{\omega} \frac{|I(\omega, t)|}{|V(\omega, t)|} \quad (39)$$

where

$$|Y_x(\omega)|^2 = \left(\frac{p^2 R_m}{R_m^2 + (1/\omega C_m - \omega L_m)^2} \right)^2 + \left(\omega C_0 + \frac{p^2 (1/\omega C_m - \omega L_m)}{R_m^2 + (1/\omega C_m - \omega L_m)^2} \right)^2 \quad (40)$$

It is natural to ask if the suboptimal control (39) is effective at approximating our true objective (38). Substituting the mechanical resonant frequency (37) into the gradient of (40) w.r.t. ω yields the optimal slope to track. That is,

$$y'_{opt} = \left. \text{grad}(|Y_x(\omega)|^2) \right|_{\omega=\omega_1} = \frac{-2\omega_1 C_0}{R_m^2} (2p^2 L_m - C_0 R_m^2) \approx \frac{-4p^2 \omega_1}{R_m^2} C_0 \quad (41)$$

Since C_0 is very small, y'_{opt} is a small negative number that in most applications that can be approximated as zero.

Solving (39), is equivalent to enforcing the heuristic, $y'_{opt} = 0$. In short, control problems (38) and (40) are related by

$$\omega^* = \arg \max_{\omega} |Y_m(\omega, t)| \approx \arg \max_{\omega} |Y_x(\omega, t)| + \frac{R_m^2 \omega_1}{2} C_0 \quad (42)$$

where the optimal drive frequency ω^* is just slightly higher than that obtained from (39).

3. EXTREMUM SEEKING CONTROL

Tracking the appropriate resonant frequency is important because the natural frequency of the device drifts over time as the USDC heats up during high power drilling. In the previous section the control objective was introduced. In the following, the details of the control algorithm are introduced. The algorithm is a real-time optimization algorithm that tracks the time-varying drift of the device. The algorithm can be broken down into two different modes—hillclimbing, estimation-based extremum-seeking control. These modes are introduced below.

3.1. Hill-climbing

The most straightforward frequency control approach is to employ hill-climbing techniques [7]. This approach drives the ultrasonic actuator at some arbitrary initial frequency ω_1 . Once the USDC reaches steady-state at this frequency, the current and voltage amplitudes are time-averaged and sampled to yield a performance function estimate $y_1 = I_1/V_1$. Increasing the number of waveforms averaged, increases the signal-to-noise ratio of this estimate while prolonging its latency. The drive frequency is then adjusted $\omega_2 = \omega_1 + h$ where h is a relatively small step-size, and the current and voltage amplitudes are sampled again to yield $y_2 = I_2/V_2$. If $y_2 > y_1$, the search direction was favorable and is used in the next iteration, i.e. $\omega_3 = \omega_2 + h$. Otherwise, the search direction is ill-advised, and we choose $\omega_3 = \omega_1 - h$. The control algorithm continues until it begins “climbing” up a resonant peak of the device. Since there are several resonant peaks to the device, it is important that ω_1 is near the desired peak to climb. Increasing the step-size increases the convergence rate to the peak. Once the peak is reached, the algorithm switches back and forth about the optimum drive frequency. Decreasing the step-size, decreases oscillations about the peak. Specifically, the fixed-step hill-climbing algorithm is implemented with the following recursive formulas

$$\begin{aligned} \omega_k &= \omega_{k-1} + dx_k \\ dy_k &= I_k/V_k - I_{k-1}/V_{k-1} \\ dx_k &= \begin{cases} h_f & , \quad dx_{k-1} > 0, dy_{k-1} > 0 \\ -h_f & , \quad dx_{k-1} \leq 0, dy_{k-1} > 0 \\ h_{rev} & , \quad dx_{k-1} \leq 0, dy_{k-1} \leq 0 \\ -h_{rev} & , \quad dx_{k-1} > 0, dy_{k-1} \leq 0 \end{cases} \end{aligned} \quad (43)$$

where $h_f > 0$ and $h_{rev} > 0$ are user-defined fixed step sizes for the forward and reverse step directions. The fixed-step hill-climbing algorithm is generally reliable in finding the resonant peak. This is due in part because it assumes nothing about the modeling parameters that describe the shape, location and drift rate of the resonant peak as the device is drilling. However, due to the fixed-step size, the commanded input frequency of the drive sinusoid tends to “jump” back and forth such that the output jumps back and forth on both sides of the resonant peak. To circumvent this problem, the fixed-step in (43) can be replaced with the following variable-step update

$$dx_k = \kappa \cdot sat\left(\frac{dy_{k-1}}{dx_{k-1}}\right) \quad (44)$$

where κ is a user-defined gain and the $sat(.)$ function clips the derivative approximation in order to keep the step-size within user-defined bounds. As the drive frequency approaches resonance, the slope of the admittance versus frequency map begins to flatten out which implies that $|dx_k| < |dx_{k-1}|$ by virtue of (44). This approach is generally effective in eliminating excessive dithering of the input frequency near resonance. A drawback of this approach is that the admittance slope is approximated using only a single point measurement which can be sensitive to noise disturbances. In order to avoid excessive switching of the sinusoidal input frequency, it is desirable to obtain a continuous estimate of the drive frequency once a sufficiently small neighborhood of the resonant peak has been identified. Towards this end, a least squares estimator is developed next.

3.2. Estimation-based extremum-seeking control

In this section, we assume that the admittance function can be approximated by a quadratic function whose parameters are identified in real-time using an online estimator. The assumed quadratic model is

$$y(t) = y_0 - a(\omega(t) - \omega_0)^2 \quad (45)$$

where $\omega(t)$ is the commanded (known) sinusoidal drive frequency at time t , and $y(t)$ is the measured electrical admittance (performance metric) of the ultrasonic transducer. The unknown, and generally time-varying parameters of this model include parameters ω_0 , y_0 and a . Clearly, if these parameters are estimated correctly in real-time (model fits the input/output data with least-squares error), then ω_0 corresponds to the resonant frequency, y_0 corresponds to the admittance at resonance and a corresponds to the curvature of the resonant peak near resonance (*provided $\omega(t)$ is within a sufficiently small neighborhood of resonance*). In order to avoid numerical conditioning problems in estimating y_0 , model (45) is rewritten in increment form [7]:

$$z(t) = 2\omega_0\Delta\omega(t) - a\Delta\omega^2(t) \quad (46)$$

where

$$z(t) = y(t) - y(t-1)$$

$$\Delta\omega(t) = \omega(t) - \omega(t-1)$$

$$\Delta\omega^2(t) = \omega^2(t) - \omega^2(t-1)$$

Equation (46) is linear in its unknown parameters, and therefore can be rewritten as

$$z(t) = \phi(t)^T \theta \quad (47)$$

where

$$\phi(t)^T = [\Delta\omega(t) \quad \Delta\omega^2(t)] \quad (48)$$

Standard least-squares algorithms can be used to minimize the following estimation error.

$$J(\theta) = \sum_{t=1}^N (z(t) - \phi(t)^T \theta)^2 + f(\theta - \hat{\theta}) \quad (49)$$

where f is some positive definite function [8]. In particular, the recursive least-squares estimator is given by

$$\hat{\theta}(t+1) = \hat{\theta}(t) + \frac{P(t-1)\phi(t)}{1 + \phi(t)^T P(t-1)\phi(t)} [z(t) - \phi(t)^T \hat{\theta}(t)] \quad (50)$$

where

$$P(t) = P(t-1) - \frac{P(t-1)\phi(t)\phi(t)^T P(t-1)}{1 + \phi(t)^T P(t-1)\phi(t)} \quad (51)$$

with $\hat{\theta}(0)$ given and $P(0)$ is any positive definite matrix. In [8], variations of this algorithm are given to incorporate forgetting factors in order to place more weight on new measurements over older ones, which is important in tracking time-varying parameters. Once the parameter estimates have converged the recursive algorithm above will continue to update the parameters so that they track their true time-varying values. Conditions for this to occur are outlined in [7,8]. In particular, the resonant frequency and resonant peak curvature of the device can be monitored in real-time by the following estimates

$$\begin{aligned} \hat{a} &= -\theta_2(t) \\ \hat{\omega}_0 &= -\frac{\theta_1(t)}{\theta_2(t)} \end{aligned} \quad (52)$$

Hence, the **estimation-based extremum-seeking controller** becomes

$$\omega(t+1) = -\frac{\theta_1(t)}{\theta_2(t)} + \omega_{pert}(t+1) \quad (52)$$

where ω_{pert} is a small perturbation, such as a low amplitude sinusoid, that is designed to satisfy the persistency of excitation condition as in [7]. In order for resonance tracking to remain stable, it is important to recognize that (52) is only used while the parameter estimates have converged, and the the drive frequency inputs ω_k have remained within a sufficiently small neighborhood of resonance for a sufficient amount of time. This is essential because we are fitting a quadratic function to a unimodal output map. Since unimodal functions are only locally quadratic near the optimal resonant frequency, our parameter estimator in equation (50) must only be incremented when the input frequencies are within the vicinity of resonance. When this is not the case, for instance, when the last three inputs create positive, not negative curvature, then these inputs are expunged from the algorithm since it is designed to detect when this occurs (Fix this paragraph.) The performance of this control approach in resonance tracking is experimentally demonstrated in the next section of the paper.

4. EXPERIMENTAL DEMONSTRATION

A LabVIEW software package was developed at JPL to implement the hill-climbing and estimation-based extremum-seeking control approaches for the USDC. LabVIEW operates on a personal computer and interfaces to a Tektronix function generator and oscilloscope via GPIB cables and commands. The function generator output is the frequency-controlled sinusoid that drives the USDC. The oscilloscope is responsible for measuring the voltage and current waveforms that drive the USDC. In order to increase the signal-to-noise ratio of the output signal, a moving average filter is implemented directly in the oscilloscope, and can be adjusted on-line in LabVIEW. LabVIEW generated data, imported to matlab yields the the closed-loop control plots described in figure (5) and (6) below.

4.1.1. Timing issues for controller implementation: 3 time-scale approach

The fastest time-scale is the ultrasonic oscillation time-scale. On a much slower time scale is the time-constant (or latency) of the moving time-average responsible for filtering out noisy output data from the fast time-scale. The slowest time-scale is the time-varying plant parameters. Moving average and RMS filters such as

$$v_{av}(t) = \frac{1}{T} \sqrt{\int_{t-T}^t v^2(\tau) d\tau} \quad (53)$$

improve signal-to-noise, at the expense of increased latency, as T is increased. The filter time-constant has to be small enough to track shifts in the resonant frequency, but large enough to filter out noise from the drill impacts. Typically, this involves an update latency of 100ms to 3000ms for high-power drilling.

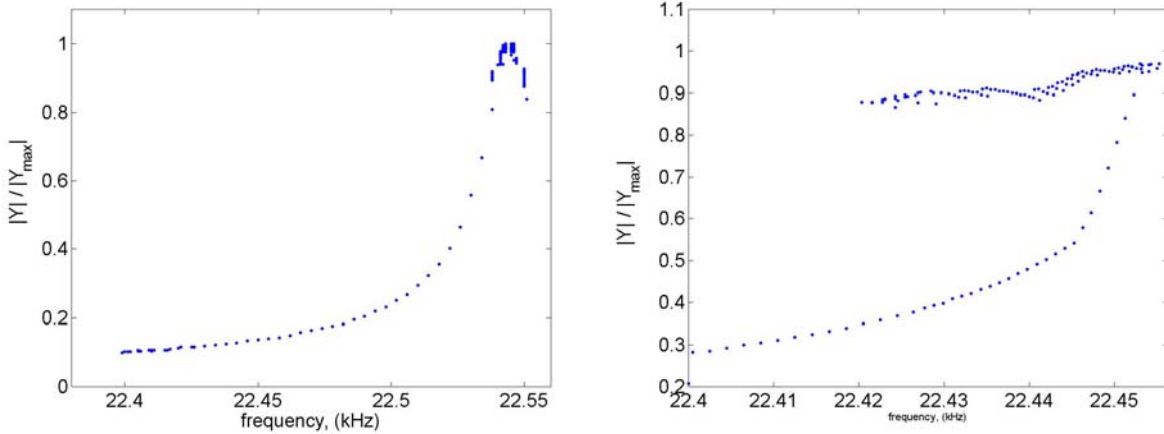


Figure 5 – Performance (admittance) v.s. input (frequency). Hill-climbing algorithm initialized at 22.4kHz. (a) Low input power increases input to 22.54kHz. (b) High input power increases input to 22.45kHz and then tracks resonance as it drops to 22.42kHz.

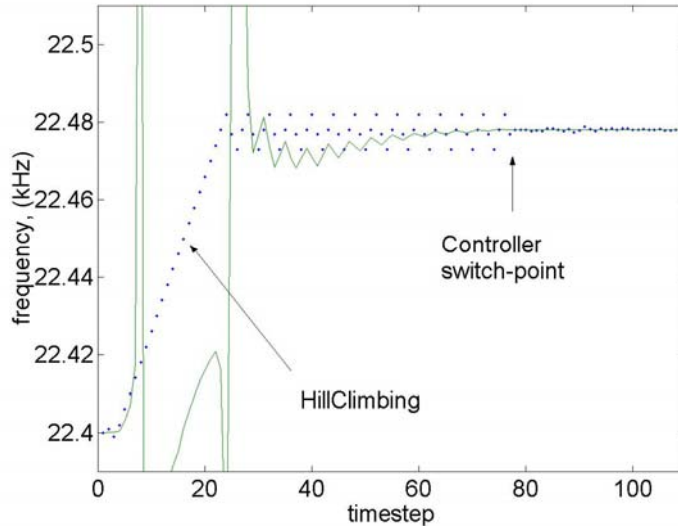


Figure 6 – Solid line represents least-squares estimate of frequency. Discrete data points are the drive frequency inputs. At the controller switch point the hill-climbing algorithm is replaced by the estimation-based extremum-seeking controller for smoother control.

5. CONCLUSIONS

Extremum-seeking control is an effective means for tracking the resonant frequency of high-power drills. The merit of this approach lies in its ability to track the resonant frequency on a time-scale that is appropriate for the drift rates of the unknown time-varying parameters. Future work will include varying the duty-cycle so that the performance can be tracked. More specifically, a variable duty-cycle can be used to ensure that the quality factor stays close to a desired level. As the USDC drills at high power, the device heats up. As the temperature in the piezoelectric elements begins to rise, the quality factor of the device decreases. Reducing the duty-cycle keeps the USDC from overheating and damaging crystals. Increasing the duty cycle reduces the time-to-drill. Typically, its both safe and efficient to run the USDC at a duty-cycle that keeps the quality factor of the device from decreasing no more than 30% of its maximal value at room-temperature. The control approach discussed next works very similar to a thermostat feedback temperature control system, with the added bonus that no temperature sensors are required, just the electrical current and voltage measurements. In particular, most thermal systems are typically governed by the following dynamical model

$$RC \frac{dT}{dt} + T = Ru \quad (53)$$

where R is the thermal resistance (Celcius*sec/kcal), and C is the thermal capacitance (kcal/Celcius), T is the current temperature (Celcius) at time t , and u is the duty cycle.

REFERENCES

1. Bar-Cohen, Y., Sherrit, S., Dolgin, B., Bao, X., Chang, Z., Krahe, R., Kroh, J., Pal, D., Du, S., Peterson, T., "Ultrasonic/Sonic Driller/Corer(USDC) for planetary application," *Proc. SPIE Smart Structure and Materials 2001*, pp. 529-551, 2001.

2. S. Sherrit, X. Bao, Z. Chang, B. Dolgin, Y. Bar-Cohen, D. Pal, J. Kroh, T. Peterson "Modeling of the ultrasonic/sonic driller/corer: USDC," 2000 IEEE Int. Ultrason. Symp. Proc., vol.1,pp. 691-694, 2000.
3. Bao, X., Bar-Cohen, Y., Chang, Z., Dolgin, B. P., Sherrit, S., Pal, D. S., Du, S., Peterson, T., "Modeling and Computer Simulation of Ultrasonic/Sonic Driller/Corer (USDC)," *IEEE Transactions on Ultrasonics, Ferroelectrics and Frequency Control (UFFC)*, Vol. 50, No. 9, pp. 1147-1160, Sept. 2003.
4. S. Sherrit, B. Dolgin, Y. Bar-Cohen, D. Pal, J. Kroh, T. Peterson, " Modeling of horns for sonic/ultrasonic applications," 1999 IEEE Int. Ultrason. Symp. Proc., pp. 647-651, 1999.
5. H. Allik and T.J.R. Hughes, "Finite Element Method for Piezoelectric Vibration," *Int. J. Num. Math. Eng.*, Vol. 2, pp. 151-157, 1970.
6. Y. Bar-Cohen, S. Sherrit, Z. Chang, L. Wesse, X. Bao, P. T. Doran, C. H. Fritsen, F. Kenig, C. P. McKay, A. Murray, and T. Peterson, "Subsurface Ice and Brine Sampling Using an Ultrasonic/Sonic Gopher for Life Detection and Characterization in the McMurdo Dry Valleys," *Proceedings of the SPIE Smart Structures Conference San Diego, CA.*, SPIE Vol. 5388-32, Mar 14-18, 2004.
7. P.E. Wellstead, P.G. Scotson, "Self-tuning extremum control," *IEE Proceedings*, Vol. 137, Pt. D, No. 3, May 1990.
8. G.C. Goodwin, K.S. Sin, "Adaptive filtering, prediction and control", Prentice Hall, New York, 1984.